Available online at www.sciencedirect.com
SCIENCE DIRECT®
Journal of Nuclear Materials 343 (2005) 92–100
journal of nuclear materials
www.elsevier.com/locate/jnucmat

Improved cavitation resistance of structural materials in pulsed liquid metal targets by surface hardening

T. Koppitz [a], P. Jung [b,*], G. Müller [c], A. Weisenburger [c], M. Futakawa [d], Y. Ikeda [d]

[a] Zentralabteilung Technologie, Forschungszentrum Jülich, D-52425 Jülich, Germany
[b] Institut für Festkörperforschung, Forschungszentrum Jülich, Jülich D-52425, Germany
[c] Institut für Hochleistungsimpuls und Mikrowellentechnik, Forschungszentrum Karlsruhe, D-76344 Eggenstein-Leopoldshafen, Germany
[d] JAERI, Tokai-mura, Ibaraki-ken 319-1195, Japan

Abstract

Cavitation damage of structural materials due to pressure waves is expected to be one of the major life-time limiting factors in high power liquid metal spallation targets under pulsed operation. Two methods are developed for the European Spallation Source (ESS) to mitigate this damage: Introduction of gas bubbles to suppress the pressure pulse, and surface hardening of structural materials to reduce their vulnerability. Surface hardening of four 8–13% Cr martensitic steels was performed by thermal treatment with pulsed or scanned electron- and laser beams as well as by nitriding in a r.f. plasma. Parametric dependences of these processes were investigated and partially optimised. Thermal treatment with electrons reached HV-hardness values up to about 600, laser treatment up to 710, and nitriding above 1200. After mechanical and metallographical characterisation, specimens of 12% Cr steel were tested in liquid mercury under pulsed proton irradiation, and under mechanical pulse-loading. Surface damage was analysed by optical, confocal laser, and scanning-electron microscopy, showing in all tests much better resistance of the hardened material compared to standard condition. Application of these techniques to a spallation target is outlined.

1. Background

Heavy liquid metal targets are considered for high power spallation sources to produce neutrons and other particles for scientific and technical applications. Especially in the case of a neutron source for condensed matter research, pulsed operation promises big advantages. But investigations under pulsed proton irradiation as well as off-beam simulation of pulsed power introduction in mercury showed already at relatively low powers severe surface damage of the target container material [1,2]. This so-called 'pitting' is ascribed to cavitation due to pressure waves. As this surface erosion is now considered to be one of the major life-time limiting factors for the target structure, methods are investigated to mitigate the pressure pulses and by this to reduce the mechanical load as well as the surface damage of the structure. The most promising method which is investigated in the ESS-project [3], is the introduction of gas bubbles, to absorb energy and increase the compressibility of the liquid. On the other hand, a general correlation

* Corresponding author. Tel.: +49 2461 614036; fax: +49 2461 614413.
E-mail address: p.jung@fz-juelich.de (P. Jung).

0022-3115/$ - see front matter © 2005 Elsevier B.V. All rights reserved.
doi:10.1016/j.jnucmat.2004.08.034

exists between hardness of materials and resistance against cavitation erosion, indicating the possibility to reduce damage by material selection. As demands for ductility, weldability, etc. exclude the application of high hardness materials for the target structure, hardening must be confined to the surface. Therefore a study has been launched on surface hardening of 9–12% Cr steels, which are prime-candidate materials for the target module in ESS. The present paper describes the applied hardening methods, resulting hardening and metallography, and effects on erosion damage under proton irradiation and off-beam pressure wave simulation.

2. Overview on surface hardening techniques

Methods for surface hardening can be roughly distinguished between those that employ chemical changes (compositional additions or coating) and homogeneous methods which use merely thermo-mechanical treatments.

2.1. Thermo-mechanical hardening methods

Hardening by *deformation* must be confined to a narrow surface region by methods such as shot peening [4], while conventional cold working would also harden the bulk of the material. In addition some steels can be hardened by *thermal treatment*, according to the multiphase Fe–C-system. For certain contents of Cr and C, hardening is achieved by lattice strains due to martensite transformation. As shown in Fig. 1 for 12% Cr DIN 1.4922, the martensite transformation starts at 250 °C (M_s) when the steel is cooling down from temperatures above A_{c1}. The low M_s-temperature of this class of steels is the reason that no fast quenching is necessary. Steels with 9–12% Cr and about 0.2% C show after austenitising a hardness of about 440 (HV30) [5,6]. By subsequent annealing, hardness drops above 550 °C to a minimum value of about 200 at 800 °C. The relatively low carbon content ($\leqslant$0.2%) of these steels limits their hardenability, but is favourable with respect to ductility, corrosion resistance (avoidance of CrC precipitation), and welding. Heating to above A_{c1} or even remelting, and subsequent cooling to M_s must be performed in a way that hardening is confined to the surface. In this process the parameters of the material, e.g. thermal conductivity and specimen thickness, and of heating, e.g. amount and duration of the heat input, must be matched to obtain the desired hardness and depth of the hardened layer.

2.2. Chemical hardening methods

Hardening of steels by *carburising* or *nitriding* is a well established method for surface hardening, for reviews cf. Refs. [7,8]. Introduction of C or N (into the

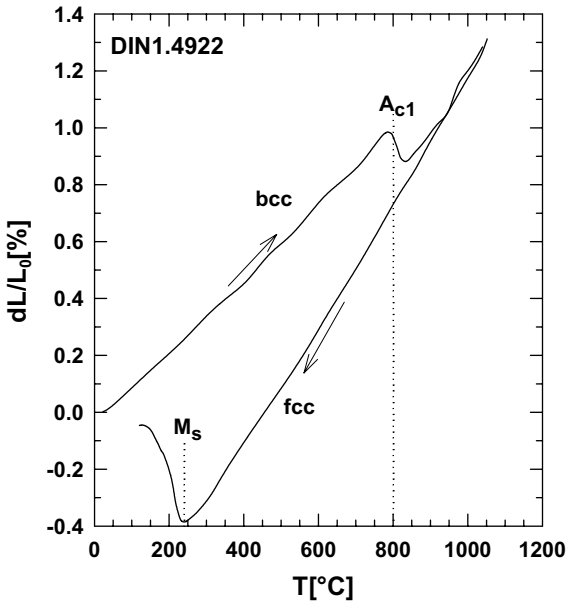

Fig. 1. Transformation diagram of DIN1.4922, measured by dilatometry. M_s and A_{c1} are transformation temperatures during cooling and heating, respectively.

%-range) into the metal can be achieved thermally from the gas phase, from a plasma, or by implantation. Low temperatures in preparation and application are mandatory to avoid carbide (e.g. CrC) or nitride precipitation with resulting reduction of corrosion resistance. Only recently plasma nitriding of martensitic steels has been developed [9]. It is generally found, that the thickness of the hardened layer increases with decreasing Cr content, increasing temperature and time, while the influence of process parameters on hardness still needs investigation. In general, nitriding is possible at lower temperatures than carburising, especially by plasma nitriding using abnormal glow discharge. Low plasma pressures allow better control of the temperature of the work piece, but at pressures below 10 Pa, plasma must be generated by r.f., by microwave or by electrons. An additional advantage of r.f. plasma is suppression of arcing and the possibility of independently applying a bias voltage which is found to accelerate nitriding and to increase hardness.

A characteristic of nitriding of high chromium steels is a plateau-type concentration- and hardness profile with a sharp edge. This can be quantitatively explained by a saturable-trap model [10], with all traps filled in the plateau region, allowing for fast diffusion of the nitrogen to the edge where it is slowed down by trapping and building up of the concentration. The height of the plateau is determined by gas pressure and plasma voltage, while depth depends on process time.

Another heterogeneous surface hardening technique is the application of hard *coatings*, e.g. of ceramic material [11]. In the case of ESS, intense pulsed irradiation, strong mechanical and thermal stresses, hot flowing mercury, and complex target geometry including joining, pose severe problems with respect to fabrication, adhesion and stability of the coatings, and would need extensive development. Therefore coatings were not included in the present study.

3. Results on surface hardening of martensitic DIN 1.4922

Two methods employing electrons were used, namely scanning of an electron-beam and pulsing of electrons from a multi-electrode source. In addition hardening by a scanned laser beam and by r.f. plasma nitriding were studied. For all methods the martensitic 12% Cr steel DIN 1.4922 was used. Nitriding was also performed on two 9% Cr steels (T91 and EUROFER97) and a 13% Cr–4% Ni steel (DIN1.4313), with compositions listed in Table 1. The DIN 1.4922 was obtained from Böhler Stahl, Kapfenberg, Austria in the form of $2800 \times 1000 \times 3.31$ mm^3 sheets (heat Nr. D70348) and of a ca. $100 \times 150 \times 200$ mm^3 bloc. The sheets were normalised for 8 min at 1022 °C in air and tempered for 4 h at 770 °C in air. They had some lamellar structure, probably from oxide inclusions during rolling, cf. Fig. 4. The material was in the fully martensitic condition. Specimens for hardening and irradiation were cut from the sheet material, while those for the off-beam erosion tests were machined from the bloc. DIN1.4313 was obtained in the form of 40 mm diameter rods from BGH Edelstahl Siegen GmbH. T91 was obtained from FZJ/IWV2 as a tube of 43×11 mm, and EUROFER97 was supplied by the European fusion programme in the form of 9 mm sheets.

3.1. Electron-beam scanning

It was intended not only to austenitise but even to melt the top of the specimen to produce a thin layer of molten steel by the heat input of the beam. This layer then solidifies in situ as a fine-grained cast on the rolled base metal. Remelting instead of solely austenitising is beneficial by homogenising of the sheet material, e.g. the lamellar structure of the DIN1.4922 sheets. Further benefits of this process are a compressive residual stress on the surface and vacuum purification of the melt. Since

Table 1
Chemical composition (wt%) of sheets (Fe bal.)

Materials	C	N	Si	P	S	V	Cr	Mn	Ni	Nb	Mo	Others
1.4922	0.22	0.032	0.29	0.020	0.004	0.26	11.21	0.66	0.64		0.91	
1.4313	0.038	0.0325	0.31	0.018	0.003		12.80	0.78	3.70		0.41	Co: 0.04
T91	0.105	0.0055	0.43	0.009		0.2	8.26	0.38	0.13	0.075	0.95	Ta: 0.1
EU-97	0.11	0.03		0.005		0.2	9.0	0.48	0.021	0.0017	<0.001	Ta: 0.07, W: 1.1

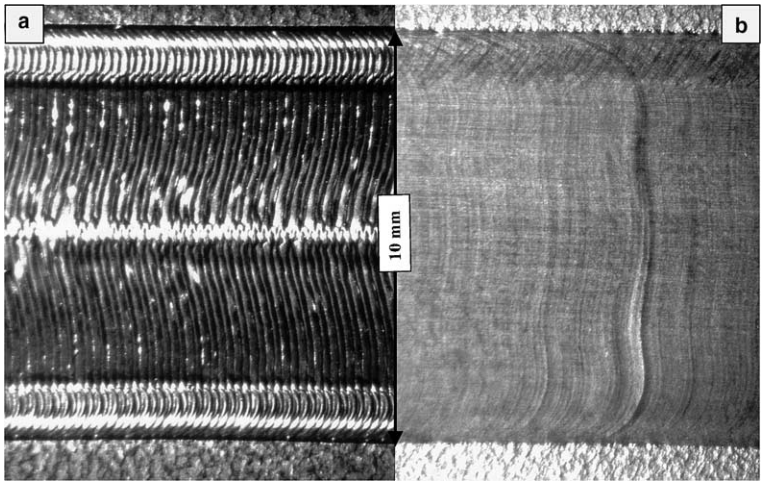

Fig. 2. Relatively rough (a) and smooth (b) surfaces, obtained by beams of 20 and 50 mA, at focus distances of 51 and 180 mm, scanned at 100 and 2000 Hz, with travel speeds of 20 and 150 mm/s, respectively.

constant heat deposition to a well defined part of the surface is most important, beam parameters (power, focus, oscillation figure, frequency) in combination with the travel speed of the work piece were optimised to obtain a plain remelted stripe of a certain width and depth. The 3.5 mm thick test specimens were clamped on a 30 mm thick copper plate to enhance self-quenching. A heat-affected zone (HAZ) between layer and base metal is hardened too, giving an ideal matching of both regions.

The electron beam was extracted from a conventional EB welding machine (EBW 300/60) at FZJ-ZAT, operated at 60 kV and $\leqslant$50 mA. The start and end positions of the beam were determined by cuboids made of tungsten. Tungsten blocks of 50–180 mm thickness were also used to focus the electron beam. When the beam was then moved to the work piece, the defocusing by these distances and the oscillation of the beam gave a remelted track of 5–11 mm width. The defocussed spot was scanned transversal to the longitudinal travel of the specimen (15–20 mm/s) with frequencies from 100 to 2000 Hz.

Surface morphologies for the beam oscillating over 10 mm in '8'-shape (more symmetric than e.g. circle) for two different sets of parameters are shown in Fig. 2. Transversal and longitudinal cross sections of the 'smooth' (Fig. 2(b)) specimen are shown in Fig. 3, indicating the dentritic structure of the solidified grains after remelting. Distribution of hardness on the cross section of the same specimen is shown in Fig. 4. Three different zones can be distinguished, each of about 200 μm thickness: A remelted zone, followed by two heat-affected zones (HAZ). Vickers hardness is highest in HAZ(1), i.e. the hardened zone (remelted area plus HAZ(1) covers a depth of about 400 μm (arrow)). The lamellar structure of the pristine material, visible as dark lines between HAZ(1) and HAZ(2) in Fig. 4, may nucleate cracks under internal stresses.

3.2. Electron beam pulsing

Two units installed at FZK/IHM (GESA-I and GESA-II) were employed to perform hardening under pulsed electron conditions. The principle layout of a

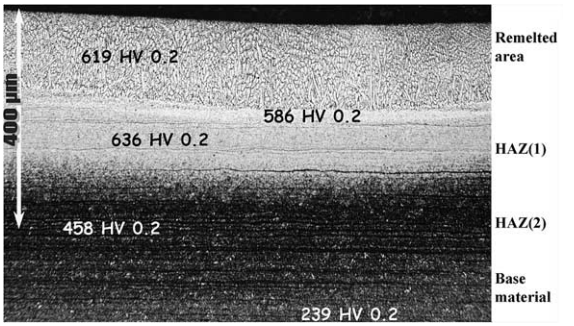

Fig. 4. Cross section with hardness measurements of the specimen from Fig. 2(b). A lamellar structure was present in the rolled sheet material, which was removed in the remelted area but prevailed in the HAZ and base material. It was not clear, whether the lines are cracks or result from preparation.

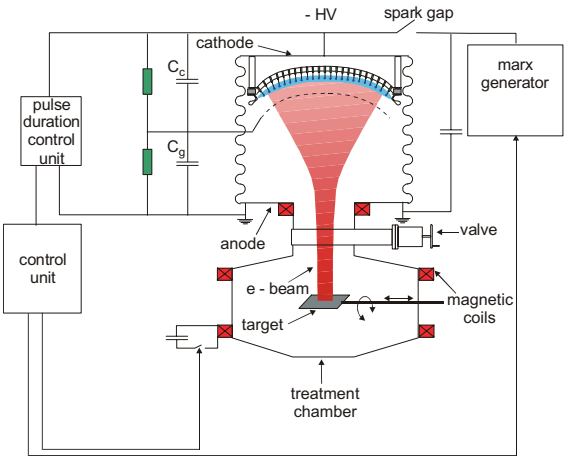

Fig. 5. Schematic view of the GESA facilities.

GESA facility is shown in Fig. 5. The main parts are: high voltage generator (marx generator) with a pulse duration control unit; electron injector (cathode); focusing magnetic coils; drift channel; chamber for sample treatment; radiation protection; control unit. The high voltage generator consists of four stages, which are

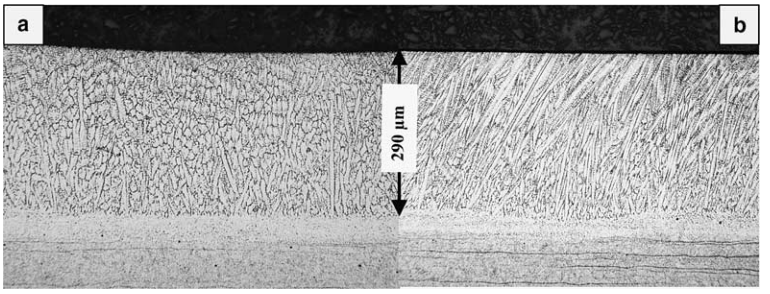

Fig. 3. Cross sections, vertical (a) and parallel (b) to the travel direction of the specimen of Fig. 2(b).

artificial pulse forming lines, containing eight cells with correcting RC networks. The electron injector consists of a high voltage insulator, a multipoint explosive emission cathode (MPC), a controlling grid and an anode, forming a triode arrangement. The MPC as electron source has a stabilized cathode plasma, which does not require heating, operates under moderate vacuum conditions, and is not poisoned by gases or vapors. The controlling grid is connected with the grounded anode through a resistor. This allows: (1) to control the beam current in a certain range without changing the kinetic energy of electrons at the outlet of the injector; (2) to create a sufficiently high electric field strength near the cathode surface at the beginning of the pulse, necessary for homogeneity of electron emission. The treatment chamber is separated from the injector volume by a gate valve for easy exchange of specimens. The residual gas pressure in the working volume is 10^{-5}–10^{-4} mbar. Parameters of the GESA facilities are listed in Table 2.

After preliminary tests on GESA-I it was found, that the higher energy of GESA-II is necessary to reach remelting to a larger depth and at a slower cooling rate. This is necessary for significant hardening of DIN1.4922, probably due to its relatively low carbon content. In a series of experiments it was tried to identify optimum parameters, such as energy, pulse duration and number of pulses, in terms of hardness, depth and surface quality.

Characteristic features were a decreasing depth of remelting from the centre to the beam periphery, and a wavy appearance of the remelted zone, mainly in the centre areas (large remelting depths). Within this wavy structure, remelting depth further varied from about 30 μm in the valleys to 160 μm on the crests, while hardness was rather constant. Sometimes a layer of lower hardness was observed on the very surface, mostly on the strongly remelted areas. It could be associated to apparent recrystallisation. Removal of this softer layer by grinding etc. is difficult due to the wavy structure. A systematic investigation of the effect of pulse length on hardness gave the depth profiles shown in Fig. 6,

Table 2
Main parameters of GESA-I and -II

Parameters	Unit	GESA-I	GESA-II
Accelerating voltage	kV	50–150	200–400
Power density	MW/cm^2	Up to 2	Up to 6
Beam diameter at target	cm	5–10	4–6
Pulse duration	μs	4–40	5–250
Cathode emission surface	cm^2	700	
Maximum remelting depth in steel	μm	50	100

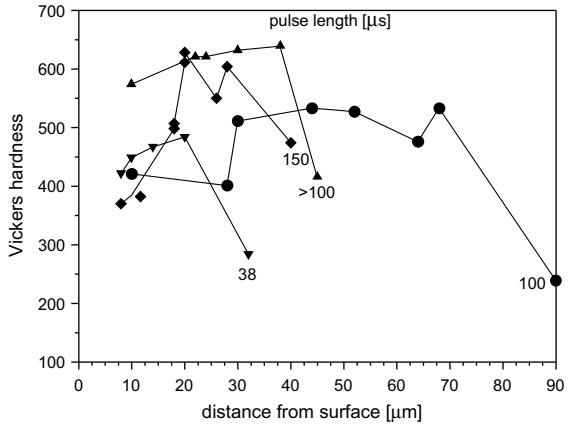

Fig. 6. Hardness profiles in DIN 1.4922 after electron pulses of 200 kV and different length from GESA-II.

yielding highest hardness values at pulse lengths between 100 and 150 μs.

A systematic investigation on the development of surface roughness and hardness on number of pulses showed that the wavy structure could be reduced somewhat by multiple pulsing. Average roughness was reduced by about a factor of about 2 after 20 pulses, while no effect on hardness was observed within statistical fluctuations. Also the surface layer with lower hardness is not significantly affected by the number of pulses. A few experiments were also performed on beam-induced alloying with aluminium by placing a thin Al foil on top of the specimen. Only in a few cases a small amount of alloyed Al could be detected in the surface, while mostly the Al was chipped off or evaporated, resulting in hardening similar to the case without Al.

An electron energy of 200 kV and pulse length of 120–150 μs seem optimum to reach Vickers hardness values between 550 and 600. Surface structure can be somewhat smoothened by repeated pulsing, but too many pulses, similar to too high energies or pulse lengths, cause recrystallisation and consequently reduction of hardness. It still has to be decided whether or not the softer layer on the surface is disadvantageous and should be removed.

Table 3
Results of plasma nitriding

Steel	Hardness of hardened layer [HV0.025]	Depth of hard layer [μm]	Width of transition region [μm]	Hardness of base metal [HV0.025]
1.4922	1220	50	30	275
1.4313	1170–1240	0–60	20	300 [HV0.05]
T91	240–1000	65	20	250
EU-97	900–1130	50	30	300

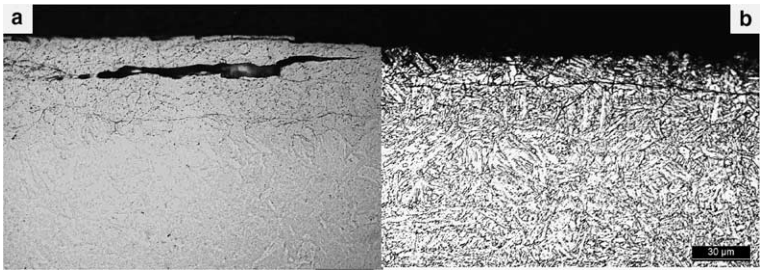

Fig. 7. Partial disintegration of plasma-nitrided layer on 9% Cr T91 (a) and 12% Cr DIN1.4922 (b) martensitic steels.

3.3. Surface hardening by laser beams[1]

Hardening by scanning of a laser beam (Nd-YAG, LAY 2006D from Trumpf comp.) was rather sensitive to surface preparation, due to the influence of reflectivity. Tests were performed on sheets of DIN1.4922 with thicknesses of 1.5 and 3.0 mm at powers from 1.5 to 2 kW, with beam cross sections from 2.4×12.2 to 4×14 mm^2, at distances from 265 to 325 mm, and scanning speeds from 3.3 to 8.3 mm/s. Cross-section measurements gave surface hardness values up to 710 (HV0.025) which decreased only smoothly with depth. HAZ ranged from 0.16 to 1.8 mm and depended strongly on cooling, which aside from surface preparation seems to be of major importance. In general, results were only poorly reproducible and variation with parameters was not sufficiently systematic to allow optimisation.

3.4. Surface hardening by plasma nitriding[2]

Nitriding was performed by r.f. plasma on sheets of about 1 mm thickness of the four different steels. Before nitriding, the surfaces were cleaned by sputtering which also caused some roughening. The subsequent cross-sectional analysis gave for all materials the same general features: A surface layer of constant high hardness and a decrease of hardness to the value of the base material within a rather narrow transition region (Table 3). The high nitrogen content in the surface region and its steep decrease caused strong internal stresses in the transition region, which sometimes causes chipping-off of the hardened layer from the cross-section specimens (Fig. 7). For this reason and because sometime cracks were starting from the edges of the Vickers indentations, mostly a load of only 0.025 was used. Other remarkable features were the large hardness fluctuations in T91, and similarly large variations in hardening depth in DIN1.4313. The (round) specimens of this steel showed some colouring, which was associated with inhomogeneous nitriding across the surface. The EU-97 showed pits of typical 0.1 mm diameter and 70 μm depth at mutual distances of about 10 mm, most astonishingly only on one side of the specimens.

4. Effect of surface hardening on cavitation erosion

Experiments on the effect of hardening on cavitation erosion were performed on DIN 1.4922 by irradiation with 0.8 GeV and by a method, producing pressure pulses mechanically.

4.1. Proton irradiation

In the irradiation period in June 2002, two flat flanges of DIN 1.4922 with 1.5 mm thickness and 130 mm diameter were irradiated in the ASTE target at WNR-LANSCE, Los Alamos [12]. One was in standard condition (HV = 250), the other was normalised for 30 min at 1040 °C and cooled rapidly in vacuum, giving HV = 500. Fig. 8 gives typical micrographs of these specimens before and after irradiation with 100 proton pulses (0.8 GeV, 2.8×10^{13} protons/pulse, 2.2 kJ, 0.3 μs). No additional pits are observed on the hardened material, when comparing identical sites of the specimen before and after irradiation. On the other, hand material in standard condition clearly showed pitting damage after irradiation.

4.2. Mechanical pressure pulse generation

The specimen flange shown in Fig. 9 was fine-polished to a surface roughness of less than 0.5 μm. Then three areas of about 60×15.5 mm each were hardened by electron pulsing with pulses of 200 kV and about 110 μs duration (Section 3.2). To remove some of the soft surface layer and to smoothen the wavy structure, the flange was slightly polished again, with typically 10–20 μm removed. This polishing was stopped when parts of the hardened areas were reached. An

[1] Hardening by laser beam was performed by Fraunhofer-Institut für Lasertechnik, Aachen under FZJ-contract Nr.132/41542169/930.

[2] Plasma nitriding was performed by ELTRO GmbH, Baesweiler under FZJ-contract Nr.240/41539956/670.

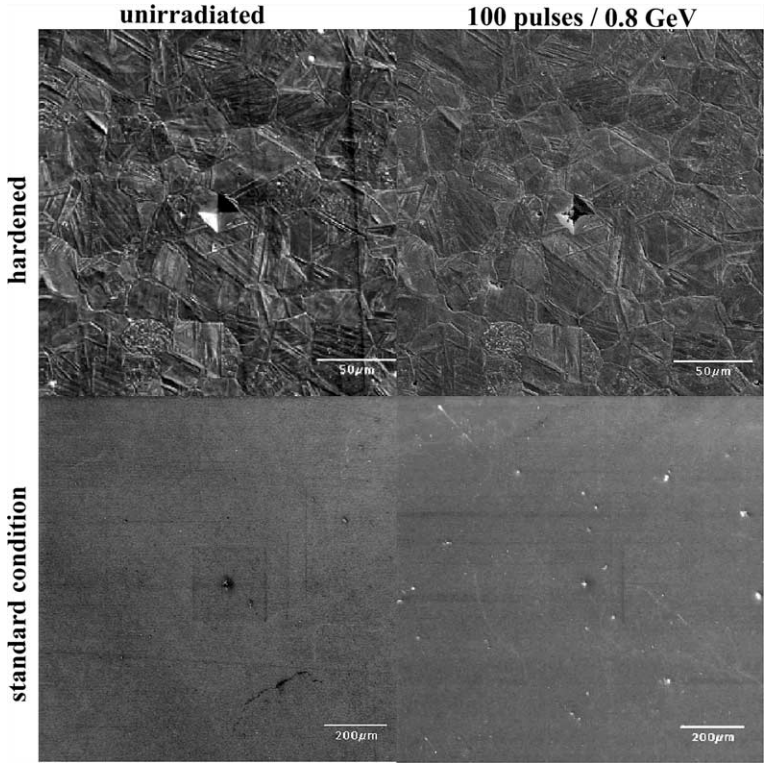

Fig. 8. DIN 1.4922 in hardened (specimen FZ-5) and standard condition (specimen FZ-6) before and after irradiation with 100 pulses of 0.8 GeV protons with 2.8×10^{13} protons per pulse.

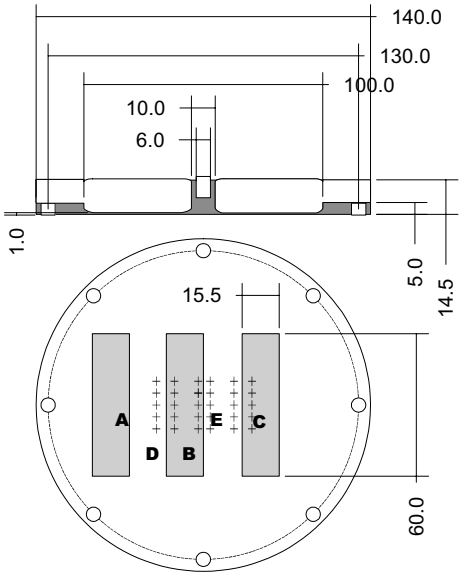

Fig. 9. Specimen flange for MIMTM facility with view of hardened areas (shaded) and test positions A, B, C, D, E. Crosses are markers for site identification.

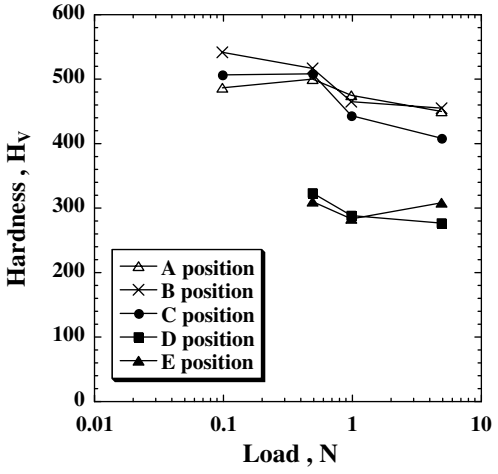

Fig. 10. Vickers hardness at four measuring sites, see Fig. 9, as a function of load.

array of 6×5 indentation markers was posed by a hardness tester at a load of 1 N. Two spots from the hardened (A, B) and from the untreated (D, E) areas were

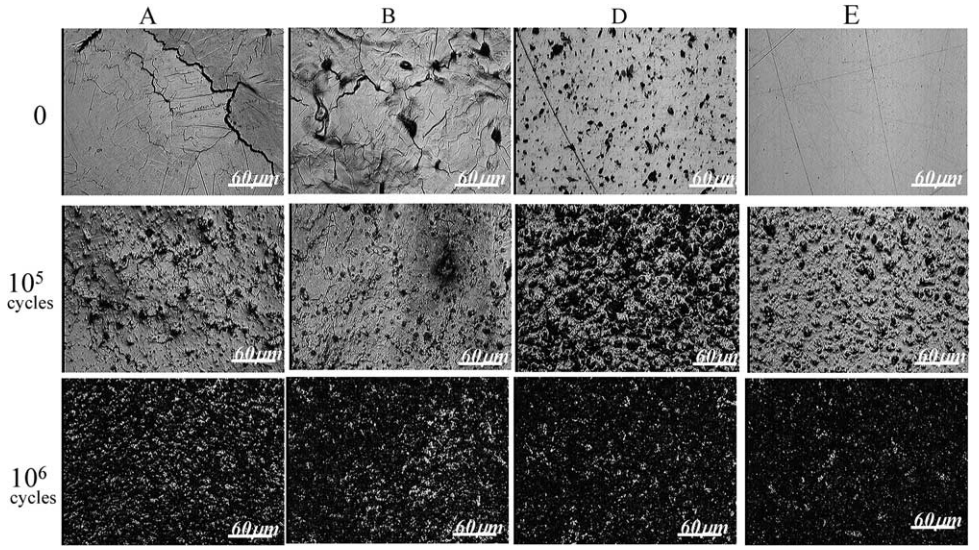

Fig. 11. Confocal laser microscopy of four measuring sited, see Fig. 9, after, 0, 10^5, and 10^6 cycles.

used for detailed analysis. Hardness values in the untreated areas averaged to about 300 HV, virtually independent of load, while the values in the hardened areas were above 500 at low loads (Fig. 10). In these regions hardness dropped with increasing load due to the limited thickness of the hardened layer. The flange was investigated in the magnetic impact testing machine (MIMTM at JAERI) [13] by pushing it against a cylindrical volume (100 mm diameter, 15 mm height) of mercury by magnetic force. The cavitation intensity exerted by this device can be adjusted by the magnet current, and corresponded in the present case to the beam power density in a typical 1 MW spallation source. Micrographs from confocal laser microscopy are shown in Fig. 11. While the untreated areas (D, E) showed smooth, polished surfaces before testing, the hardened areas (A, B) had wavy surfaces with small cracks and sometimes kind of small droplets.

The fraction of eroded area (A_e/A_0) for the four spots is shown in Fig. 12 as a function of the number of cycles N_c. The data are fitted to

$$A_e/A_0 = 1 - \exp(CN_c), \tag{1}$$

where C is a constant. The values N_c^* for which A_e/A_0 reaches 0.98, are plotted in Fig. 13 for each imposed power on MIMTM. Up to $A_e/A_0 \approx 1$ the mean depth of erosion is only slightly increasing, while above this value it increases according to about $N_c^{1.3}$ [14]. Data for austenitic 316 stainless steel in solution annealed, in kolsterised,[3] and in nitrided condition are included for comparison. It can be seen that DIN 1.4922 in standard condition allows by a factor of about five higher cycles than 316, while hardening gives another factor of about 5, approaching the values of kolsterised 316. For the austenitic 316 SS in standard and nitrided conditions, N_c^* was determined as a function of pulse power, yielding approximately a 4th power relationship [14], see Fig. 13. Similarities in pitting damage by the WNR irradiations and in MIMTM were used to relate the power density in MIMTM to that in a spallation source. If this relation is adopted for the hardened DIN 1.4922, only about 10^3 cycles would be acceptable at the typical power density in the 5 MW ESS source.

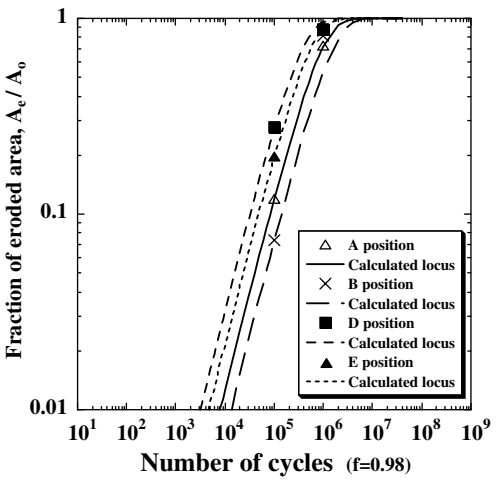

Fig. 12. Fraction of eroded area as a function of cycles and fits to Eq. (1).

[3] Kolsterising is a registered trademark of the Bodycote Company, Bodycode Hardiff BV, NL-7333 PA Appeldoorn, cf. Ref. [15].

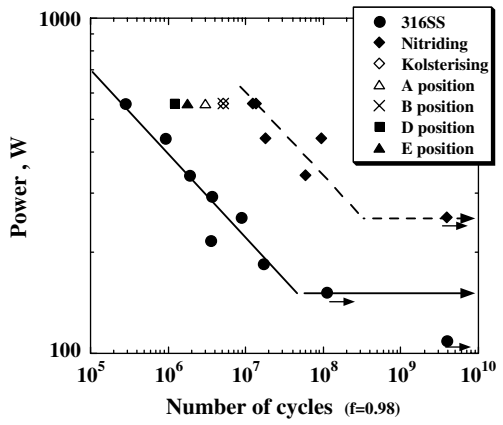

Fig. 13. Estimation (from MIMTM results) of the onset number of cycles of enhanced surface erosion, scaled for powers of spallation sources as indicated.

5. Conclusions

- Thermal treatment of 12%Cr steels gives HV values of about 600.
- Surface hardening by plasma nitriding of 8–13%Cr steels gives HV values above 1200.
- Thermally treated material shows reduction of cavitation erosion under pulsed proton irradiation as well as under mechanical loading in mercury.
- Extrapolation of these results shows that life-time also of hardened material would be limited to unacceptable low values in the ESS target.
- The effect of surface hardening on high cycle fatigue behaviour needs more investigation.
- More information on the stability of hardened surfaces under irradiation is needed.

Acknowledgement

Hardening by laser beam was performed by G. Vitr and N. Pirch from Fraunhofer Institut für Lasertechnik, Aachen, plasma nitriding by U. Huchel from ELTRO GmbH, Baesweiler. The authors are indebted to H. Soltner and H. Conrad from the ESS project and to B.W. Riemer and J.D. Hunn from the SNS project for irradiation and analysis of the targets in the LANSCE-WNR experiments in June 2002, and to T. Naoe of JAERI for assistance with the MIMTM experiments.

References

[1] M. Futakawa, H. Kogawa, R. Hino, H. Date, H. Takeishi, Int. J. Imp. Eng. 28 (2003) 123.
[2] J.D. Hunn, B.W. Riemer, C.C. Tsai, J. Nucl. Mater. 318 (2003) 102.
[3] H. Soltner, Gas bubble admixture for pressure pulse mitigation in high-power liquid–mercury spallation targets, Report ESS, 2004.
[4] International Conference on Shot Peening, Garmisch-Partenkirchen, 2002.
[5] K. Ehrlich, Formulation of initial design equations for type 1.4914 martensitic steel, Kernforschungszentrum Karlsruhe, 1986.
[6] R. Lindau, M. Schirra, Workshop on data base evaluation of RAFM steels, Brasimone, 27–28 November 2000.
[7] K. Ichii, in: T. Bell, K. Akamatsu (Eds.), Stainless Steel 2000, MANEY, Leeds, 2001.
[8] T. Bell, Y. Sun, in: T. Bell, K. Akamatsu (Eds.), Stainless Steel 2000, MANEY, Leeds, 2001.
[9] S.K. Kim, J.S. Yoo, J.M. Priest, M.P. Fewell, in: T. Bell, K. Akamatsu (Eds.), Stainless Steel 2000, MANEY, Leeds, 2001.
[10] S. Parascandola, W. Möller, D.L. Williamson, in: T. Bell, K. Akamatsu (Eds.), Stainless Steel 2000, MANEY, Leeds, 2001, p. 201.
[11] D.L. Smith, J. Konys, T. Muroga, V. Evirkin, J. Nucl. Mater. 307–311 (2002) 1314.
[12] B.W. Riemer, J.R. Haines, J.D. Hunn, D.C. Lousteau, T.J. McManamy, C.C. Tsai, J. Nucl. Mater. 318 (2003) 92.
[13] M. Futakawa, T. Naoe, H. Kogawa, C.C. Tsai, Y. Ikeda, J. Nucl. Sci. Tech. 40–11 (2003) 895.
[14] M. Futakawa, T. Naoe, C.C. Tsai, H. Kogawara, S. Ishikura, Y. Ikeda, H. Soyama, H. Date, in: 5th Internation Symposium on Cavitation, Osaka, 2003.
[15] R.H. van der Jagt, in: T. Bell, K. Akamatsu (Eds.), Stainless Steel 2000, MANEY, Leeds, 2001.